NeuroImage **17,** 77–94 (2002)
doi:10.1006/nimg.2002.1136

Virtual *in Vivo* Interactive Dissection of White Matter Fasciculi in the Human Brain

Marco Catani,*,† Robert J. Howard,* Sinisa Pajevic,‡ and Derek K. Jones*,§

**Section of Old Age Psychiatry, Institute of Psychiatry, De Crespigny Park, London SE5 8AF, United Kingdom; †Institute of Gerontology and Geriatrics, University of Perugia, Perugia, Italy; ‡Mathematical and Statistical Computing Laboratory, Center for Information Technology (MSCL/CIT), National Institutes of Health, Bethesda, Maryland; and §Division of Medical Physics, Leicester Royal Infirmary, Infirmary Square, Leicester LE1 5WW, United Kingdom*

Received December 10, 2001

This work reports the use of diffusion tensor magnetic resonance tractography to visualize the three-dimensional (3D) structure of the major white matter fasciculi within living human brain. Specifically, we applied this technique to visualize *in vivo* (i) the superior longitudinal (arcuate) fasciculus, (ii) the inferior longitudinal fasciculus, (iii) the superior fronto-occipital (subcallosal) fasciculus, (iv) the inferior fronto-occipital fasciculus, (v) the uncinate fasciculus, (vi) the cingulum, (vii) the anterior commissure, (viii) the corpus callosum, (ix) the internal capsule, and (x) the fornix. These fasciculi were first isolated and were then interactively displayed as a 3D-rendered object. The virtual tract maps obtained *in vivo* using this approach were faithful to the classical descriptions of white matter anatomy that have previously been documented in postmortem studies. Since we have been able to interactively delineate and visualize white matter fasciculi over their entire length *in vivo*, in a manner that has only previously been possible by histological means, "virtual *in vivo* interactive dissection" (VIVID) adds a new dimension to anatomical descriptions of the living human brain. © 2002 Elsevier Science (USA)

Key Words: **white matter; fasciculi; tractography; diffusion tensor; MRI; VIVID.**

INTRODUCTION

Since the end of the 19th century, delineation and description of the architecture of the human brain has been an active area of research, and a variety of techniques to assist in visualizing the network of connections that are integral to brain function have been developed.

Dejerine (1895, 1901), in a classical work on neuroanatomy, studied histological sections of brain tissue in which the myelin had been Weigert-stained and produced a detailed atlas of neuroanatomy in which the course of major fibers in white matter was depicted in a series of two-dimensional (2D) figures. The Klingler technique of freezing the brain prior to dissection (Ludwig and Klingler, 1956) has permitted three-dimensional (3D) visualization of the trajectories of certain white matter fasciculi. Techniques have been developed to study the route of particular fibers by exploiting active axonal transport of exogenous tracer materials including horseradish peroxidase and radioactive tracers (Cowan and Cuénod, 1975; Heimer and Robards, 1981; Heimer and Záborszky, 1989), but the requisition for active transport means that these techniques are clearly unsuitable for study of the human brain. A further technique that shows great promise for the study and visualization of white matter tracts *in vitro* has recently been proposed by Axer *et al.* (2000). Polarized light is passed through a histological section of tissue and subsequently through a second polarizer. By examining the extent to which the birefringence of myelin bends some of the light, and therefore allows light to pass through the pair of polarizers, the orientation of fibers can be estimated.

All of these methods, however, are necessarily invasive and therefore unsuitable for the study of living human subjects in a clinical environment. In this work, we delineate different white matter fasciculi using a noninvasive approach that uses magnetic resonance imaging and exploits differences in the self-diffusivity of water in different regions of the brain.

In fluid-filled regions, such as the CSF-filled ventricles, the self-diffusivity of water is the same in all directions. In gray matter, the diffusion of water molecules is more hindered due to the presence of cell membranes, macromolecules, and so forth. At the typical resolution of magnetic resonance (MR) data (e.g., $2 \times 2 \times 2$ mm), the self-diffusivity of water in gray matter appears to be the same in all directions (i.e., it is "isotropic"), but is reduced compared to the self-diffusivity of CSF in the ventricles. However, in white matter, the diffusivity of water molecules is much less hindered along the long axes of ordered axons than

1053-8119/02 $35.00

perpendicular to the long axes, where molecules take a more tortuous route. In this situation, the diffusivity is not the same in all directions (i.e., it is "anisotropic"). The self-diffusivity of water in an anisotropic system such as the white matter cannot be adequately described by a single scalar quantity and can be described only by a diffusion tensor—a symmetric matrix with six unique elements that fully characterizes the diffusion process (Crank, 1956).

Basser *et al.* (1994) showed how this self-diffusion tensor could be estimated noninvasively in each voxel of a MR image data set, with a technique now known as diffusion tensor MRI (DT-MRI). In brief, a series of MR images that are sensitized to diffusion in different directions (by applying diffusion-encoding gradients) are collected, and a model is fitted to the data to estimate the diffusion tensor in each voxel. For each voxel, it is then possible to calculate the trace, which provides a rotationally invariant estimate of diffusivity (Basser *et al.*, 1994), various measures of diffusion anisotropy (Basser *et al.*, 1994; Basser and Pierpaoli, 1996; Pierpaoli and Basser, 1996), which reflect the degree of tissue structure, and the orientation of the diffusion tensor (Basser and Pierpaoli, 1995), which has been shown to be parallel to the dominant orientation of anisotropic structures *in vivo*.

By estimating the diffusion tensor in each voxel, and subsequently its orientation, it is possible to estimate and display the principal orientation of anisotropic structures *in vivo*, and several methods have been developed for achieving this (Coremans *et al.*, 1994; Basser and Pierpaoli, 1995; Nakada and Matsuwaza, 1995; Ulug *et al.*, 1996; Jones *et al.*, 1997; Pierpaoli, 1997; Pajevic and Pierpaoli, 1999, 2000).

Makris *et al.* (1997) used color-coded fiber orientation images (derived from DT-MRI data), combined with *a priori* knowledge of the location and pathways of white matter fasciculi, to produce a series of two-dimensional coronal images within which the major fasciculi were identified. The individual fasciculi were clearly delineated due to abrupt changes in fiber orientation at the boundaries of fasciculi, and the authors demonstrated correlation between color-coded fiber orientation images and an anatomical map of the human brain (Dejerine, 1895, 1901), highlighting the potential of using DT-MRI to study the morphometry of white matter fasciculi. However, visualization of the three-dimensional morphometry of a particular fasciculus in its entirety using data presented solely in a two-dimensional format is difficult.

A rapidly emerging technique in the field of DT-MRI is that of fiber tracking or "tractography" (Basser, 1998; Jones *et al.*, 1998, 1999a; Mori *et al.*, 1999; Poupon *et al.*, 1999, 2000; Conturo *et al.*, 1999; Basser *et al.*, 2000). The aim of tractography is to reconstruct the 3D trajectories of white matter tracts, generally by following a continuous path of greatest diffusivity (i.e., least hindrance to diffusion) through the brain from an initial set of "seedpoints."

Three-dimensional reconstruction of tracts by tractography makes identification of the pathways of white matter much easier than by a 2D slice-by-slice format (such as color-coded fiber orientation maps)—as recently demonstrated by Stieltjes *et al.* (2001) in the cerebral peduncles/brainstem. Here we have adopted a similar strategy to attempt to elucidate the 3D morphometry of 10 major white matter fasciculi, as determined by diffusion tensor MR tractography.

The aim of this work is not to introduce a new tractography method *per se*, but to show how a combination of an optimized data acquisition protocol (Jones *et al.*, 2002), an existing tractography method (Basser *et al.*, 2000), and a visualization approach (Zhang *et al.*, 2000), when used in conjunction with preexisting knowledge of neuroanatomy, can be used to perform virtual gross anatomical dissections of nerve pathways that bear striking resemblance to classical neuroanatomical descriptions, in a clinically feasible time period.

METHOD

Data Acquisition

Diffusion-weighted magnetic resonance imaging data were acquired from a healthy male volunteer (39 years of age and free of neurological symptoms), on a 1.5 T GE Signa NV/i LX system (General, Electric, Milwaukee, WI) with actively shielded magnetic field gradients (maximum amplitude 40 mT m^{-1}). A standard quadrature birdcage head coil was used for both RF transmission and NMR signal reception.

The subject's consent was obtained, according to the declaration of Helsinki, and the scanning protocol was approved by the local Ethical Committee at our institution.

Data were acquired using a multislice peripherally gated EPI sequence, optimized for precise measurement of the self-diffusion tensor in the human brain (Jones *et al.*, 1999b,c), from 60 contiguous near-axial slice locations with isotropic ($2.5 \times 2.5 \times 2.5$ mm) resolution. The echo time was 107 ms while the effective repetition time was 15 R–R intervals. The duration of the diffusion-encoding gradients was 17.3 ms, giving a maximum diffusion weighting of 1300 s mm^{-2}. Diffusion gradients were applied in 64 isotropically distributed orientations (Jones *et al.*, 1999c). An independent study (Skare *et al.*, 2000) carefully compared various diffusion-encoding gradient schemes and concluded that the method employed in the current study (Jones *et al.*, 1999c) resulted in higher-precision estimates of the diffusion tensor than any of the others. The total data acquisition time was 14 min. More complete details can be found in Jones *et al.* (2002).

Diffusion Tensor Data Analysis

Data were analyzed on an independent workstation (Sun Sparcstation Ultra 140; Sun Microsystems, Mountain View, CA). The diffusion-weighted images were initially corrected for the effects of eddy-current-induced distortion using in-house software. A reference image was first constructed by calculating the mean intensity in each voxel from all the non-diffusion-weighted images. Next, for each diffusion-weighted image the downhill simplex method (Press *et al.*, 1992) was used to select the optimal magnification, shear, and displacement of the diffusion-weighted images to give the best registration with the reference image. The "mutual information" (Studholme *et al.*, 1997) was used to assess the registration between the "reference" image and the corrected image.

Following correction of image distortion, the diffusion tensor was calculated for each voxel using multivariate linear regression after logarithmic transformation of the signal intensities (Basser *et al.*, 1994). The fractional anisotropy of the tensor in each voxel was subsequently determined, and a multislice fractional anisotropy image (Basser and Pierpaoli, 1996) was created.

The data acquisition strategy employed in this work produced a series of *discrete* estimates of the diffusion tensor field on a regular grid (i.e., at the center of each image voxel).

The next step in data analysis involved generating a *continuous* approximation of the diffusion tensor field from the discrete (voxelwise) measurements, using the B-spline-based continuous tensor field approach described by Aldroubi and Basser (1999) and Pajevic *et al.* (2001). Essentially, this allows an estimate of the tensor field to be obtained at any arbitrary point within the imaged region, i.e., not just at the center of an image voxel, by fitting a series of mathematical functions to the data. One of the effects of noise in the MR imaging system is to introduce uncertainty in the estimate of the orientation of the diffusion tensor. This problem was partly ameliorated in this work by imposing a slight smoothness constraint on the tensor field, as described by Aldroubi and Basser (1999) and Pajevic *et al.* (2001).

Tractography Algorithm

The software for estimating and reconstructing the trajectories of tracts from DT-MRI, based on the procedure originally described by Basser (1998), was written in the "C" programming language. A set of locations for the initiation of the tracking algorithm (referred to here as "seedpoints") was first selected on the fractional anisotropy images (see below). For each of these seedpoints, the orientation of the diffusion tensor was estimated. The tracking algorithm then moved a distance of 0.5 mm along this direction. The diffusion tensor at this new location was determined from the *continuous* description of the tensor field (Aldroubi and Basser, 1999; Pajevic *et al.*, 2001) and its orientation subsequently estimated. The algorithm then moved a further 0.5 mm along this direction. A pathway was traced out in this manner until the fractional anisotropy of the tensor fell below an arbitrary threshold (set to 0.15 in this case). The procedure was then repeated by tracking in the direction opposite to that of the first step at the seedpoint, to reconstruct the whole tract passing through the seedpoint (Basser, 1998; Basser *et al.*, 2000).

Seedpoint Selection

As suggested above, the first step toward generating images of fasciculi was to define suitable starting regions for the tracking procedure. By careful reference to classical neuroanatomical works (Dejerine, 1895, 1901; Ludwig and Klingler, 1956) and textbooks (Crosby *et al.*, 1962; Nieuwenhuys *et al.*, 1988), 3D regions of interests (ROIs) that were believed to contain a section of the fasciculus of interest were defined on the anisotropy images (using one or more slices).

The dispim image display program (David Plummer, Medical Physics Department, University College Hospital, London—http://www.medphys.ucl.ac.uk) was used to visualize the anisotropy data and define ROIs. A homegrown program written in "C" determined the coordinates of all voxels contained within the region of interest.

Two different approaches were used for "*in vivo* dissection." A "one-region of interest" approach was used for fasciculi whose boundaries were clearly delineated on the fractional anisotropy image. For example, there are no other fasciculi in the neighborhood of the central portion of the corpus callosum and it was straightforward to define a single ROI such that only fibers belonging to the corpus callosum were included. However, it is known from classical neuroanatomy studies (e.g., Dejerine, 1895, 1901; Ludwig and Klingler, 1956; Crosby *et al.*, 1962) that cerebral white matter is mainly composed of different fasciculi that run closely to one another. In such cases, it is difficult to place a single region of interest on the anisotropy image that includes only the fibers of only one of the fasciculi. To overcome this problem, we adopted a "two-regions of interest" approach, in a manner similar to that suggested by Conturo *et al.* (1999). The procedure was to define a second ROI, at a distance from the first ROI, such that it contained at least a section of the desired fasciculus but did not contain any fibers of the undesired fasciculi that passed through the first ROI. The placement of the ROIs (whether using a one-region or two-regions-of interest approach) was an iterative and interactive procedure. As stated in the Introduction, our aim was to demonstrate the use of preexisting

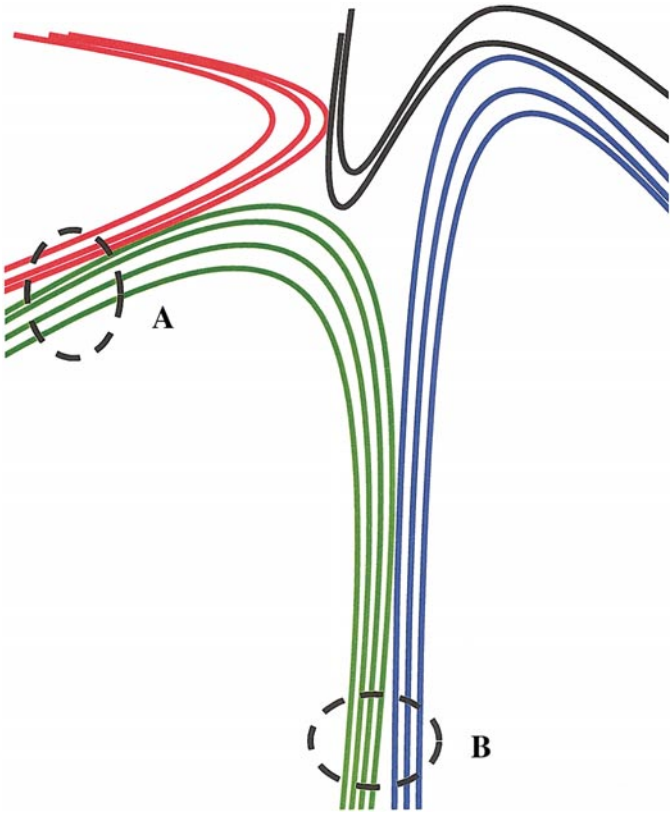

FIG. 1. Example of the use of the "two-regions of interest" approach to separate a particular fasciculus. In the illustration, the fasciculus of interest is shown in green. Region of interest A includes tracts belonging to the red fasciculus, while region of interest B includes tracts belonging to the blue fasciculus—none of which are required. The green fasciculus passes through both regions and is therefore retained for display, when employing the "two-regions of interest" approach.

technology to produce virtual gross dissection of white matter fasiculi. In a manner similar to that of a dissectionist who would carefully choose where to "cut" based on his neuroanatomical knowledge, to get a clean dissection, the "tractographer" in this study iteratively chose the ROI locations so as to obtain clean and faithful "virtual dissections" of white matter fasciculi.

Figure 1 illustrates this approach schematically. In this case, the fasciculus of interest is shown in green. If a single ROI were to be used, e.g., region A, then although the region was drawn to contain the fasciculus of interest, it is clear that some fibers belonging to the red fasciculus would also be included. To avoid this, a very small ROI could be selected—but this would be at the risk of excluding some fibers belonging to the fasciculus of interest. Region of interest B has been drawn where, *a priori*, it is known that the green fasciculus will pass through. Again, fibers from another fasciculus (shown in blue) have been included within this second ROI. If tracking were initiated from either of the regions A or B as shown, then paths belonging to multiple fasciculi would be picked up. However, by retaining only those tracts whose paths connect both regions of interest, it is possible to select exclusively those fibers that belong to the desired fasciculus. In this way, with careful cross-referencing to neuroanatomical works, any fasciculus of interest can be "dissected" from others. This approach was found to isolate fasciculi of interest very reliably.

To increase the number of pathways that could be tracked from a particular ROI, an option to create multiple seedpoints within each voxel was included in the tracking software. This was done by subdividing each voxel into a set of smaller cubes and placing a seedpoint at the center of each cube. Figure 2 shows a two-dimensional representation of the placement of initiation sites for different "dither" factors. For a dither factor of 1, tracking is initiated from only one location (seedpoint) within the voxel. Whereas, for example, if a dither factor of 2 is used, tracking is initiated from eight (i.e., $2 \times 2 \times 2$) seedpoints within the voxel.

The fasciculi studied, using this approach, were (i) the superior longitudinal (arcuate) fasciculus, (ii) the inferior longitudinal fasciculus, (iii) the superior fronto-occipital (subcallosal) fasciculus, (iv) the inferior fronto-occipital fasciculus, (v) the uncinate fasciculus, (vi) the cingulum, (vii) the anterior commisure, (viii) the corpus callosum, (ix) the internal capsule, and (x) the fornix.

The one-region of interest approach was used for the superior longitudinal fasciculus, the cingulum, the fornix, and the corpus callosum, while the two-regions of interest approach was used for the remaining fasciculi.

Typical computation time for computation of trajectories from 100 seedpoints was 20 s, running on a Sun Sparcstation Ultra 140 (Sun Microsystems).

Display of Derived Tracts

At the end of the tracking procedure, a set of points which lay at 0.5-mm intervals along the pathway of each tract was generated. To create a 3D representation of the pathways, a set of polygonal prisms with circular cross section and fixed radius were generated to connect the points, and lighting appropriate for giv-

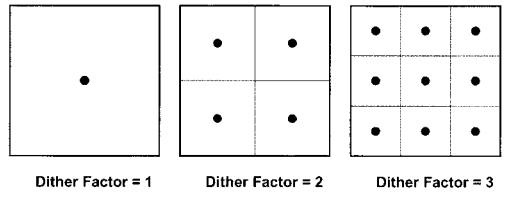

FIG. 2. 2D representation of placement of seedpoints within a voxel for three different dither factors, producing 1, 8, and 27 seedpoints per voxel.

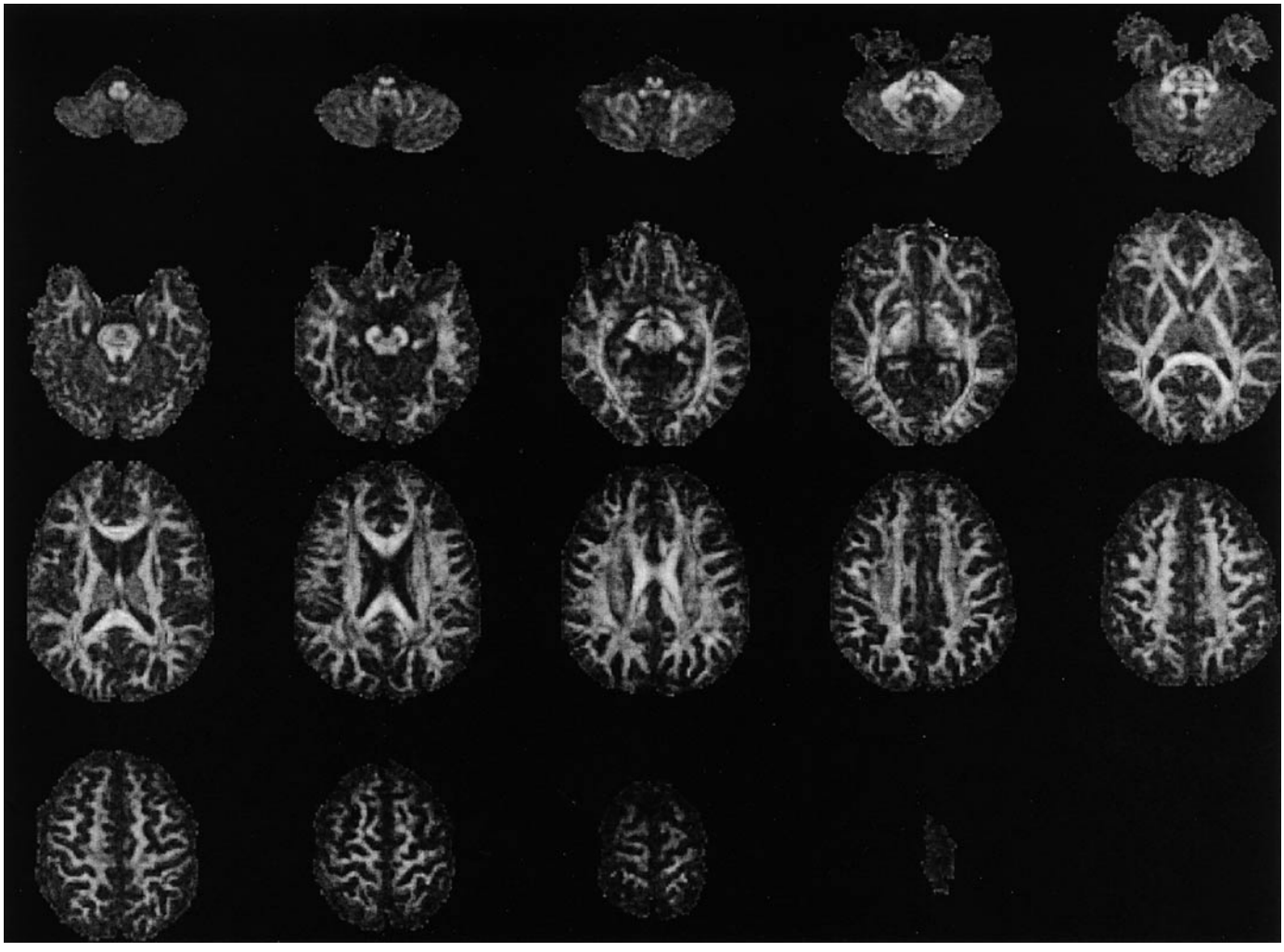

FIG. 3. Fractional anisotropy data obtained in subject (male, 39 years). Every third slice is shown from a 60-slice data set. The intensity is directly proportional to the anisotropy. While the location of anisotropic white matter can be determined, it is not possible to discern the pathways of individual fascicles from this scalar image.

ing a satisfactory image of the fasciculi was added, using the mathematical software package MATLAB (The Mathworks, Natick, MA). (The use of "streamtubes" for the visualization of white matter trajectories in this way was first reported by Zhang *et al.* (2000)). The rendered data could be rotated about all three axes to permit viewing of the tracts from any angle. In some cases, to serve as a frame of reference when viewing the derived tracts, the fractional anisotropy data were interpolated to 1.5-mm isotropic resolution and resliced in appropriate orientations.

RESULTS

Figure 3 shows every third slice from the fractional anisotropy image data set obtained from the subject. The image intensity is directly proportional to the anisotropy. Note that in the fluid-filled ventricles, the intensity is low—reflecting isotropic diffusion. White matter structures are hyperintense, reflecting the highly organized structure of the tissue. However, it is not possible to identify individual fasciculi within this image, where fasciculi run close to each other.

A result obtained using the two-ROI approach to separate two different fasciculi, the inferior fronto-occipital fasciculus and the uncinate fasciculus is given in Fig. 4. The placement of the ROIs is also shown on the accompanying axial anisotropy slices, together with an indication of the level of the axial slices on the sagittal image. Since it was known *a priori* (Dejerine, 1895; Crosby *et al.*, 1962) that the two fasciculi pass close to one another at the level of the anterior floor of the external capsule (Fig. 4 slice 1), the same ROI was used for initiation of tracking for both. To dissect the tracts of the occipito-frontal fasciculus, a second region of interest was placed posteriorly (Fig. 4 slice 2 & 3), while to track the uncinate fasciculus, an inferior ROI was selected (Fig. 4 slice 4).

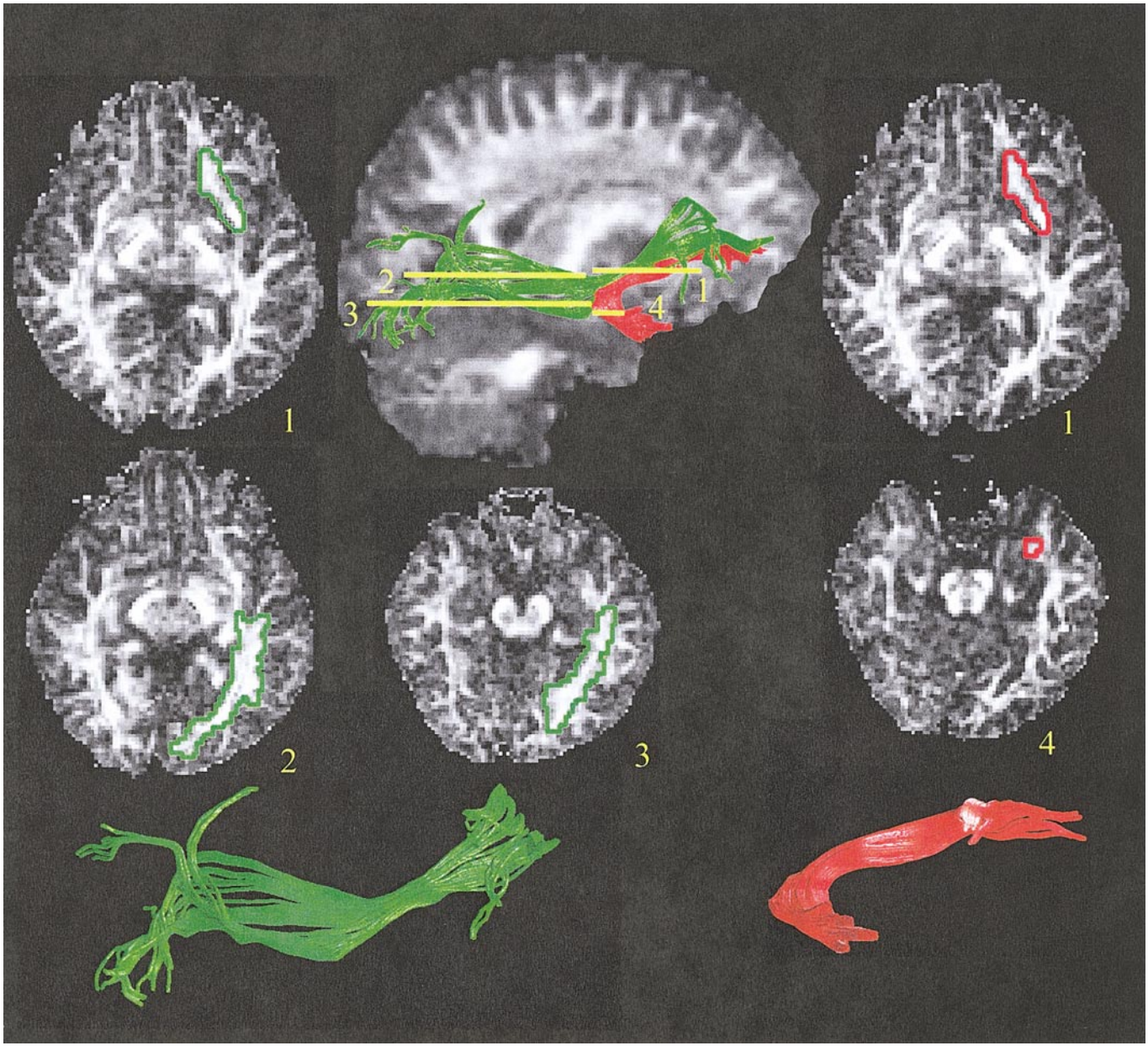

FIG. 4. Example of "*in vivo* dissection" of the occipito-frontal fasciculus from the uncinate fasciculus using the two-ROI approach. The first ROI was placed in slice 1, where the fibers of both fasciculi are enclosed. The second ROI for the uncinate fasciculus was placed more inferiorly (slice 4), whereas the second ROI for the inferior fronto-occipital fasciculus was placed more posteriorly. The sagittal slice illustrates the positions of the axial slices. Reconstructed fasciculi and regions of interest for the fronto-occipital and uncinate fasciculi are shown in green and red, respectively.

We now present results from virtual *in vivo* dissection of the major white matter fasciculi, together with a description of their pathways, origins, and terminations. While fasciculi were visualized in both hemispheres, we present here results in one hemisphere for each fasciculus, for clarity.

Long Association (Intrahemispheric) Fibers

Superior longitudinal (arcuate) fasciculus. This is the largest of the fiber bundles (Klingler and Gloor, 1960; Williams and Worwick, 1980) that together with the uncinate and fronto-occipital fasciculi constitute the longitudinal association fiber system that connects each frontal lobe with its respective hemisphere (Gloor, 1997; Kiernan, 1998). Figure 5 shows three different views of the trajectory of the superior longitudinal fasciculus (SLF) obtained by tractography. The SLF connects perisylvian frontal, parietal, and temporal cortex and can be broadly divided into (i) longer fibers which run medially within the fasciculus and connect

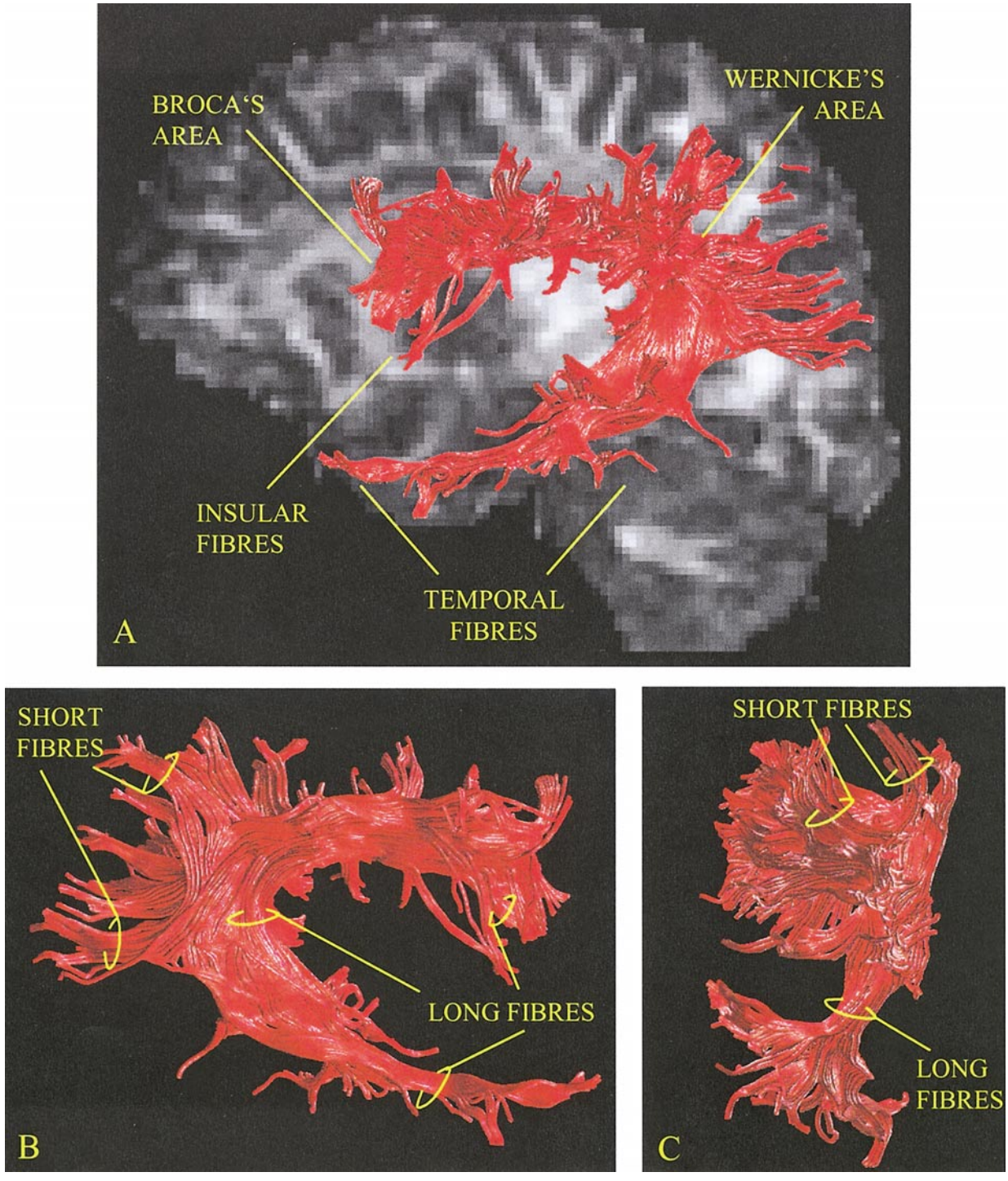

FIG. 5. The superior longitudinal fasciculus (left hemisphere) is a long associative bundle composed of long and short fibers that connect the frontal lobe with the parietal, occipital, and temporal lobes. The short fibers are best visualized in the lateral view of the parasagittal section (A) and in the posterior view of the coronal section (C), whereas the long fibers are best viewed in the medial view of the parasagittal section (B). (A) Lateral view of parasagittal section; (B) medial view of parasagittal section; (C) posterior view of coronal section.

lateral frontal cortex with dorsolateral parietal and temporal cortex and (ii) shorter U-shaped fibers which run more laterally to connect fronto-parietal, parieto-occipital, and parieto-temporal cortex (Dejerine, 1895; Crosby *et al.*, 1962; Williams and Worwick, 1980; Nieuwenhuys *et al.*, 1988). Fibers originate in prefrontal and premotor gyri (mainly Broca's area) and project posteriorly to Wernicke's area (and occipital lobe) be-

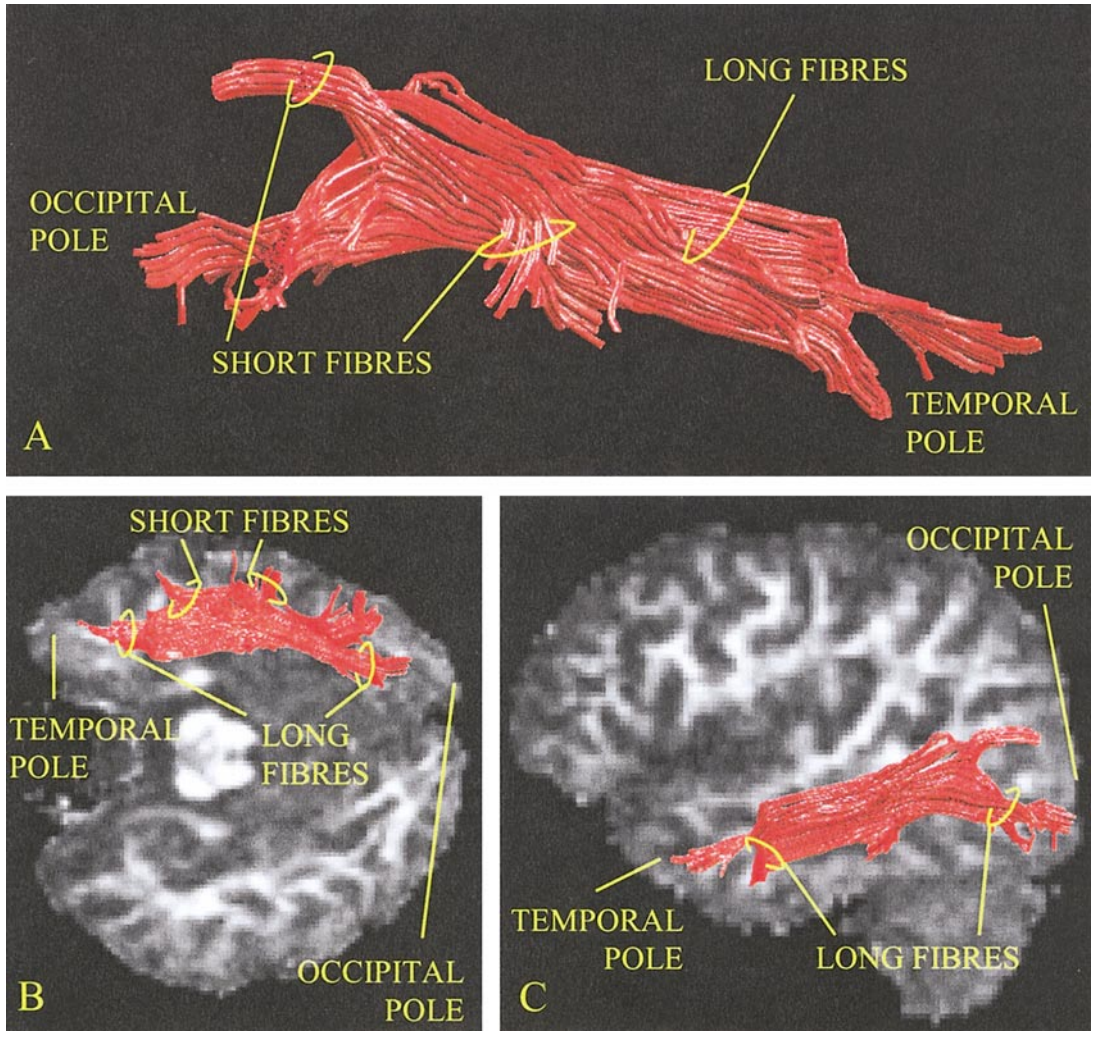

FIG. 6. The inferior longitudinal fasciculus (right hemisphere) runs through the temporal lobe, connecting the temporal pole with the occipital pole (long fibers). The short fibers emerge from nonpolar temporal and occipital areas and connect neighboring gyri. (A) Lateral view of the parasagittal projection; (B) superior view of the transversal section; (C) medial view of the parasagittal section.

fore arching around the insula and putamen to run anteroinferiorly toward the temporal pole (Dejerine, 1895; Crosby *et al.*, 1962; Williams and Worwick, 1980; Lee Seldon, 1985; Petrides and Pandya, 1988; Nieuwenhuys *et al.*, 1988; Kiernan, 1998). In addition, a small number of fibers originate in the insula of Reil and project to the cortex of the other lobes (Mesulam and Mufson, 1985; Lee Seldon, 1985).

Inferior longitudinal fasciculus. The inferior longitudinal fasciculus connects the temporal lobe with the occipital lobe (Dejerine, 1895). Figure 6 shows fibers arising in the superior, middle, and inferior temporal and fusiform gyri and projecting to the lingula, cuneus, lateral surface of the occipital lobe and occipital pole (Dejerine, 1895; Crosby *et al.*, 1962). The tract passes along the lateral wall of the occipital and temporal horns of the lateral ventricle. In the human brain the inferior longitudinal fasciculus contains mainly long association fibers but also carries some shorter cortico-cortical fibers (Gloor, 1997). In nonhuman primates most of the fibers in this tract are very short cortico-cortical fibers and this has led to the renaming of this tract as the occipito-temporal projection system (Tusa and Ungerleider, 1985).

Superior fronto-occipital (subcallosal) fasciculus. Although the components of this bundle are not well characterized it has been considered to carry fibers that connect occipital and temporal regions with frontal cortex and insula of Reil (Crosby *et al.*, 1962). Although the tractography algorithm produced an image that faithfully followed the textbook description of the frontal component (Fig. 7), the posterior projections were different. In our images, the superior fronto-occipital fasciculus appears to connect mainly dorsolateral prefrontal cortex with the superior parietal gyrus. This in accord with some earlier representations of the

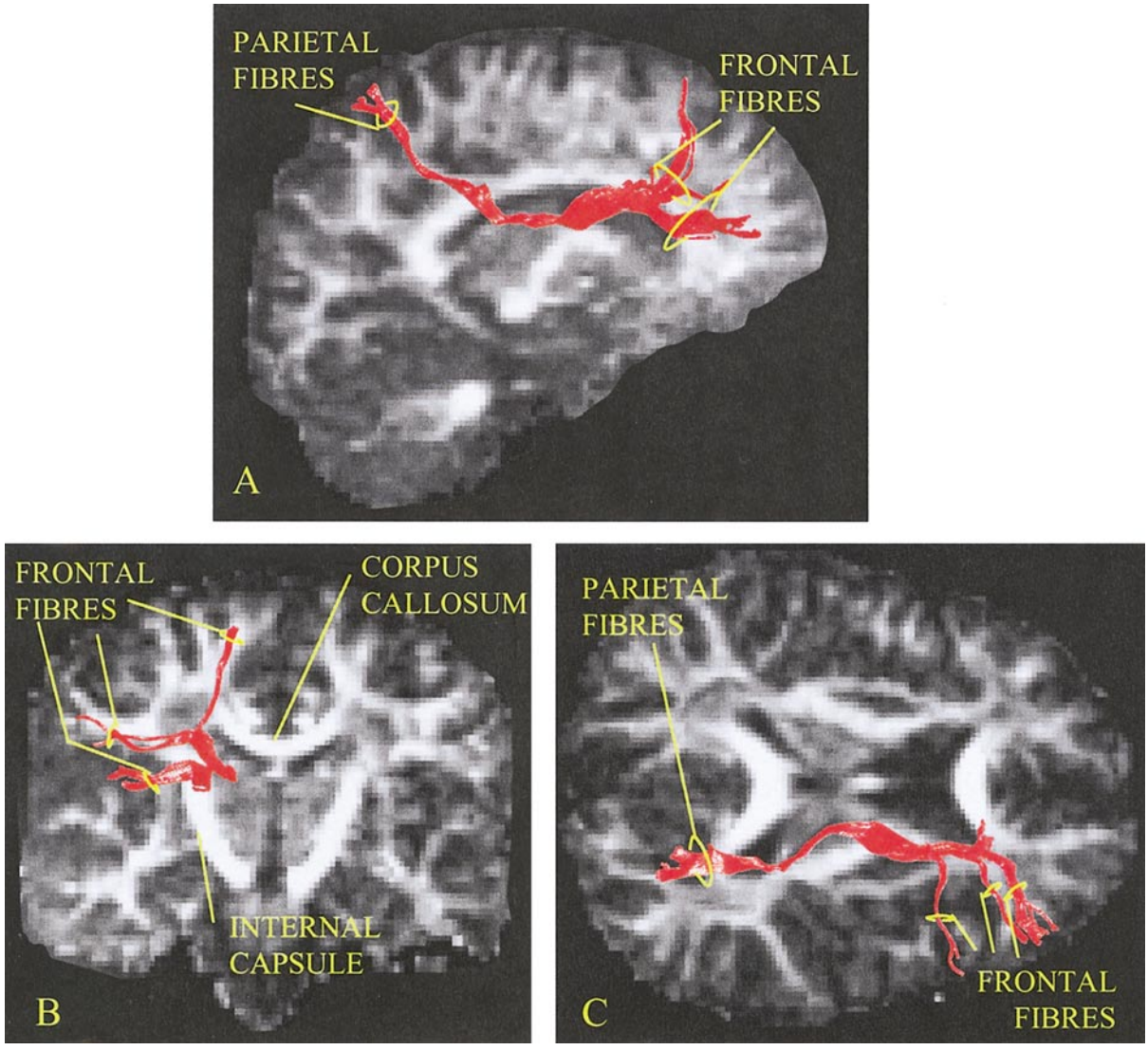

FIG. 7. The superior fronto-occipital fasciculus (right hemisphere) is a long association bundle whose posterior terminations are not well characterized. The tractography result presented here is at variance with some classical neuroanatomical studies. In the lateral view of the parasagittal section (A), the fibers seem to terminate in the parietal lobe rather than in the occipital lobe. The location of the fasciculus between the commissural fibers of the corpus callosum and the projection fibers of the internal capsule is clearly visualized in the coronal section (B). (A) Lateral view of parasagittal section; (B) coronal section; (C) superior view of the transversal section.

tract (for example Fig. 282, Crosby *et al.*, 1962; Fig. 215.1, Nieuwenhuys *et al.*, 1988), but the name of the fasciculus implies a more posterior projection. Fibers arising in the lateral prefrontal cortex of the inferior and middle frontal gyri, join to form a tight bundle at the level of the anterior horn of the lateral ventricle (Dejerine, 1895). The tract then runs posteriorly, superolateral to the caudate, and can be easily seen in coronal sections at the apex of the lateral ventricle (Dejerine, 1895; Crosby *et al.*, 1962; Nieuwenhuys *et al.*, 1988). Fibers continue to run posteriorly lateral to the lateral ventricle before turning to run postero-superiorly to terminate in the superior parietal gyrus.

Inferior fronto-occipital fasciculus. Figure 8 shows the tractography result obtained in the inferior fronto-occipital fasciculus which connects infero-lateral and dorso-lateral frontal cortex with posterior temporal cortex and the occipital lobe (Crosby *et al.*, 1962; Gloor, 1997). The fasciculus runs posteriorly from mainly prefrontal cortical areas immediately superior to the uncinate in the frontal lobe (Nieuwenhuys *et al.*, 1988). At the junction of the frontal and temporal lobes, the fasciculus narrows in section as it passes through the anterior floor of the external capsule. As the uncinate hooks away anteromedially, the inferior fronto-occipital fasciculus continues posteriorly before radiating to

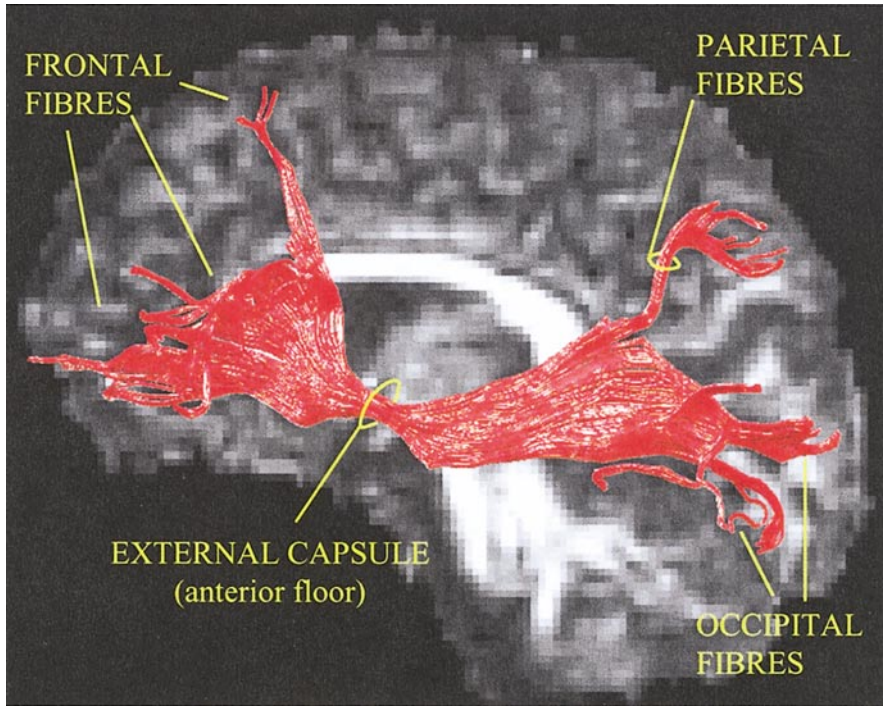

FIG. 8. Lateral view of the parasagittal section of the left inferior fronto-occipital fasciculus. The inferior fronto-occipital fasciculus is a bow-tie-shaped bundle that runs medially in the temporal lobe and inferiorly in the frontal lobe. The fibers of the inferior fronto-occipital fasciculus compact in the anterior floor of the external capsule where they run parallel to the more inferior fibers of the uncinate fasciculus.

the occipital lobe. These radiations terminate in the middle and inferior temporal gyri and in the lingual and fusiform gyri within posterior temporal and inferior occipital cortex (Crosby *et al.*, 1962; Nieuwenhuys *et al.*, 1988).

Uncinate fasciculus. The uncinate fasciculus connects the anterior part of the temporal lobe with orbital and polar frontal cortex. In the tractography result presented in Fig. 9, dorsal and more lateral fibers from the frontal pole run posteriorly to join with a more

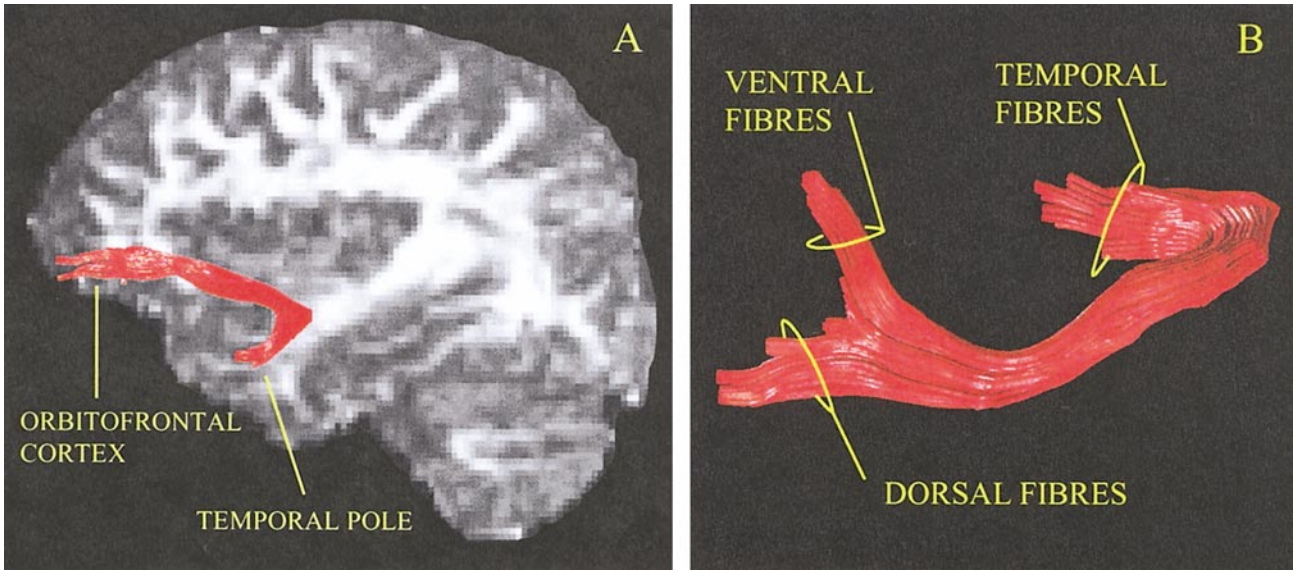

FIG. 9. The uncinate fasciculus (left) connects the temporal pole to the orbitofrontal cortex. The frontal fibers from the medial (ventral component) and the lateral orbitofrontal cortex join to form a single compact bundle that arches inferiorly toward the temporal polar region. (A) Lateral view of the parasagittal section; (B) superior view of a transversal projection.

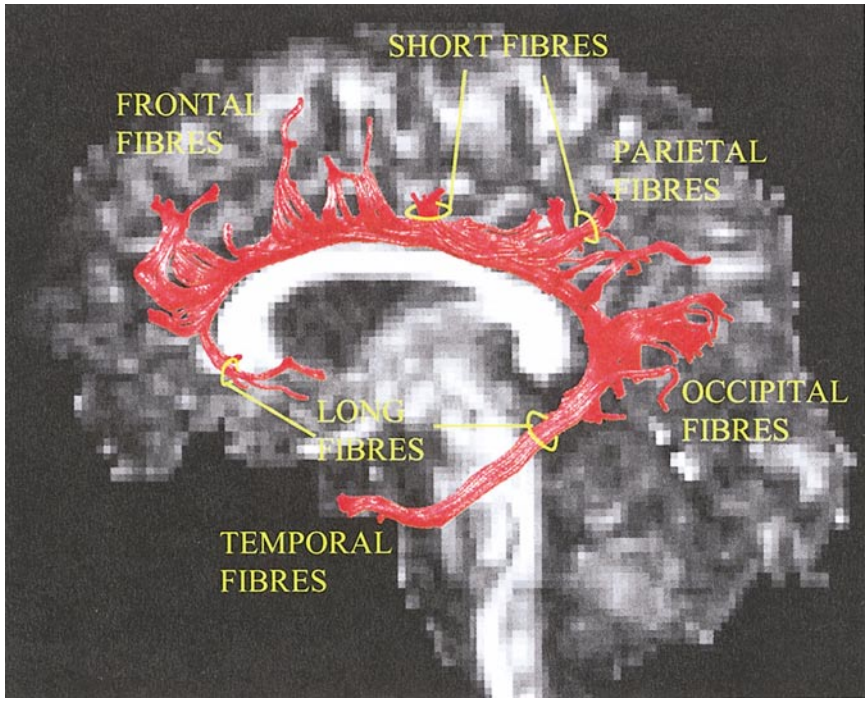

FIG. 10. Lateral view of the left cingulum. The long fibers connect the frontal lobe to the temporal lobe, whereas the short fibers connect neighboring areas of the cingulate and medial gyri of the frontal, parietal, occipital, and temporal lobes.

ventral and medial "division" from orbital cortex to form the uncinate (Dejerine, 1895; Crosby *et al.*, 1962). This runs for a short length inferior to the fronto-occipital fasciculus before entering the temporal lobe as a single compact bundle within which the two divisions can still be distinguished. The uncinate then hooks round anteromedially to terminate in the temporal pole, uncus, hippocampal gyrus, and amygdala (Crosby *et al.*, 1962; Kingler and Gloor, 1960).

The cingulum. Figure 10 shows a lateral view of the reconstructed trajectory of the cingulum. The cingulum contains fibers of different lengths, the longest of which run from the uncus and parahippocampal gyrus to subrostral areas of the frontal lobe (Crosby *et al.*, 1962; Nieuwenhuys *et al.*, 1988). From the uncus, the cingulum runs posteriorly to arch through almost 180 degrees around the splenium to constitute most of the white matter of the cingulate gyrus. It then extends around the genu of the corpus callosum to the subcallosal gyrus and the paraolfactory area of Broca (Crosby *et al.*, 1962). Shorter fibers, that join and leave the cingulum along its length, connect medial frontal gyrus, posterior parietal lobule, and the cingulate, cuneate, lingual, and fusiform gyri (Dejerine, 1895; Nieuwenhuys *et al.*, 1988).

Commissural (Interhemispheric) Fibers

The anterior commissure. The anterior commissure is a bundle of fibers shaped like the handlebars of a bicycle and straddling the midline (England and Wakely, 1991). Two types of fibers are recognized within the tractography result presented in Fig. 11: more anterior fibers connecting the olfactory bulb, anterior perforated substance, and anterior olfactory nucleus and more posterior fibers connecting the amygdala, hippocampal gyrus, and inferior temporal and occipital cortex (Crosby *et al.*, 1962; England and Wakely, 1991; Di Virgilio *et al.*, 1999). The olfactory fibers are said to be exceedingly small in primates (Lauer, 1945; Kiernan, 1998) and were not visualized in our images. The nonolfactory fibers can be further subdivided into more anterior and more posterior subdivisions. The more anterior of these connect the amygdala (Turner *et al.*, 1979) and temporal pole (Demeter *et al.*, 1990), while the more posterior connect middle and inferior temporal gyri, parahippocampal region, and fusiform gyri (Crosby *et al.*, 1962; Pandya and Rosene, 1985). The anterior commissure also receives fibers from the inferior occipital cortex in man, but not in macaque (Di Virgilio *et al.*, 1999; Rockland and Pandya, 1986). The anterior commissure is a familiar landmark on sagittal conventional MR images (Mai *et al.*, 1997) where it crosses the midline as a compact cylindrical bundle between anterior and posterior columns of the fornix beneath the septum pellucidum and anterior to the third ventricle (Dejerine, 1895). After crossing the midline, the tract runs laterally at first through the perforated substance and between the glo-

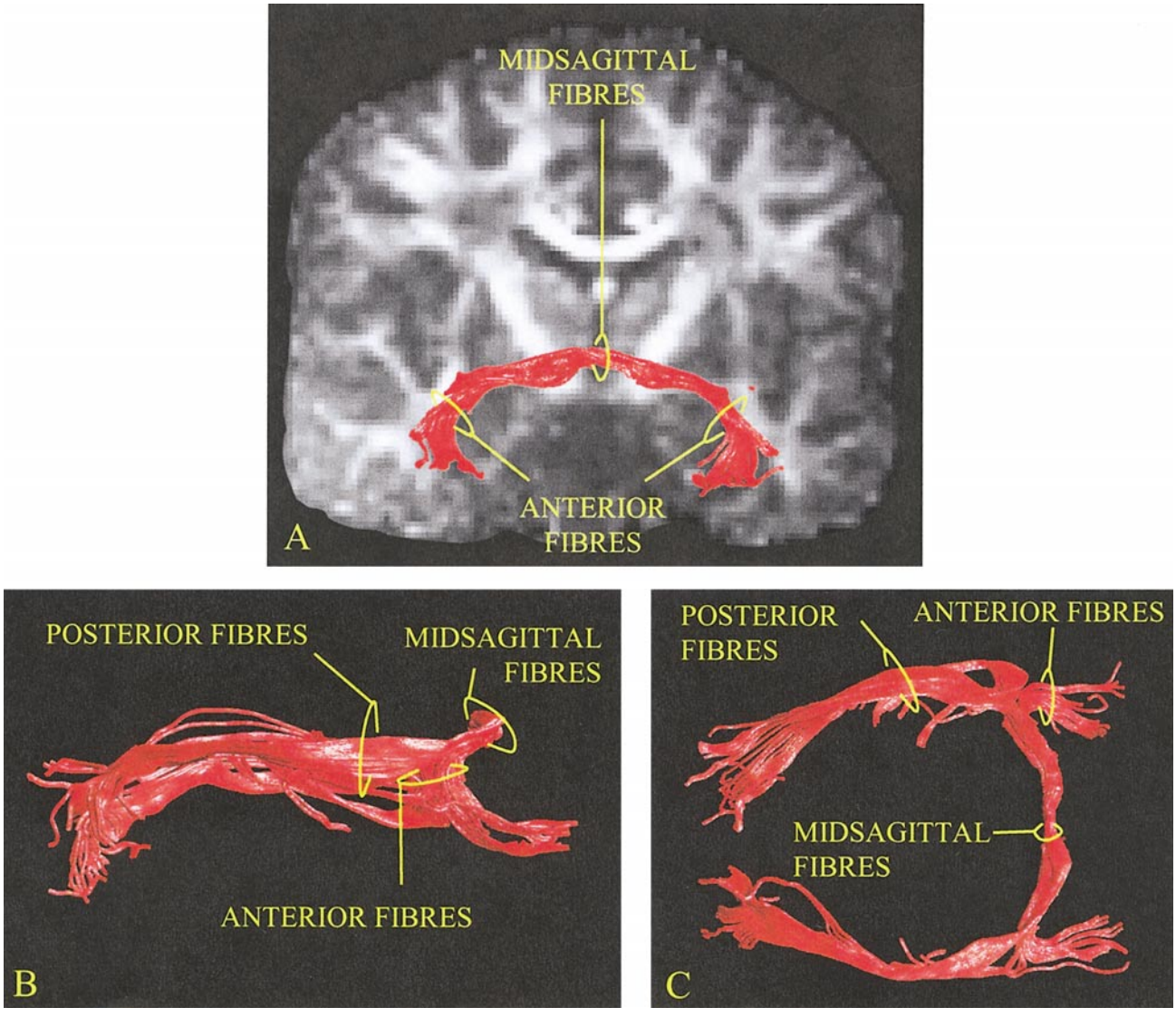

FIG. 11. The anterior commissure connects the amygdala and temporal pole (anterior fibers) and mainly the inferior temporo-occipital cortex (posterior fibers). Its fibers cross the midline as a compact bundle (midsagittal fibers) but divide into two components as they enter the temporal lobe. (A) Anterior view of coronal projection; (B) lateral view of sagittal projection; (C) superior view of transversal projection.

bus pallidus and the putamen before dividing (Dejerine, 1895). The more posterior division runs parallel to the inferior longitudinal fasciculus toward the temporo-occipital junction while the more anterior division follows the course of the uncinate fasciculus into the anterior temporal lobe.

The corpus callosum. The corpus callosum connects the major neopallial portions of the two hemispheres (Dejerine, 1895). The results of tractography performed in the corpus callosum are shown in Fig. 12, where it is seen that fibers originate in the cortex of all the hemispheres' lobes and converge at the midline to form a compact bundle that forms the roof of the lateral ventricle and continues to the contralateral hemisphere (Dejerine, 1895). In the midline the corpus callosum is divided into an anterior portion (rostrum and genu), a middle portion (body), and a posterior portion (splenium) (Crosby *et al.*, 1962). The rostrum and genu connect anterior parts of the frontal lobes (mainly prefrontal) and their horseshoe-shaped radiating fibers form the anterior (minor) forceps (Nieuwenhuys *et al.*, 1988; England and Wakely, 1991). The genu contains fibers from orbital, medial, and dorsal frontal cortex. These fibers cross the corona radiata and converge toward the anterior horn of the lateral ventricle where they form a compact bundle that arches in the genu. The body contains fibers that connect the premotor and precentral frontal cortex (rostral and middle parts of the body of the corpus callosum, respectively); the parietal lobe (middle part) and the temporal lobes (the more posterior parts) (Nieuwenhuys *et al.*, 1988). These fibers converge at the posterior horn of the lateral ventricle, around which they

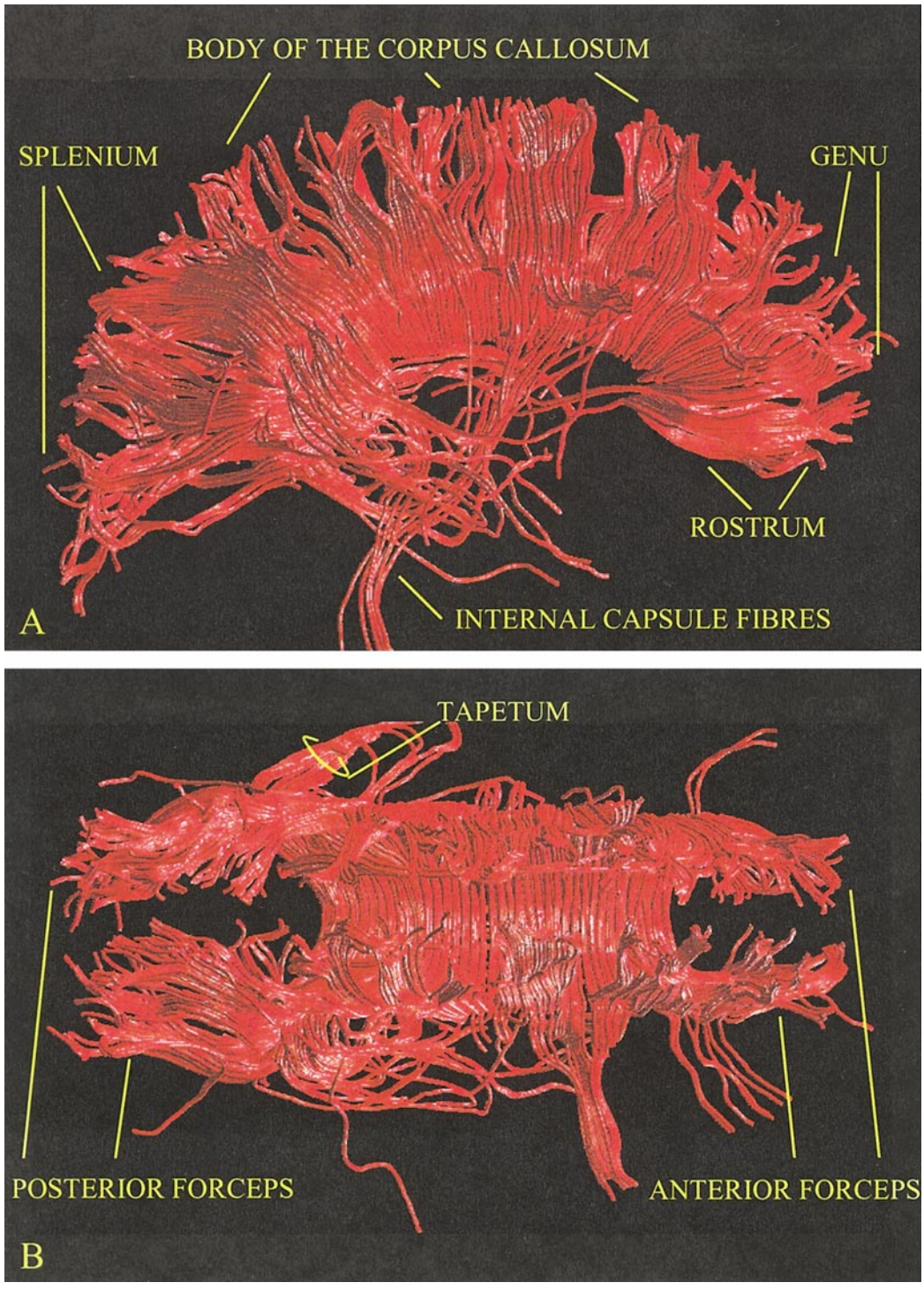

FIG. 12. The corpus callosum joins the cortex of both cerebral hemispheres. It is conventionally divided into an anterior portion (genu and rostrum), central portion (body), and posterior portion (splenium and tapetum). The fibers of the genu and the rostrum arch anteriorly to form the anterior forceps, while those of the splenium form the posterior forceps. Note that some fibers of the corpus callosum cross the longitudinal fissure and enter into the internal capsule (heterotopic fibers). (A) Lateral view of sagittal projection; (B) superior view of transversal projection.

are shaped like a cone, before arching medially to cross the midline. Fibers from the splenium make up the posterior (major) forceps. A group of fibers in the splenium known as the tapetum sweep inferiorly over the inferior horn of the lateral ventricle to connect the temporal lobes (Dejerine, 1895; Crosby *et al.*, 1962).

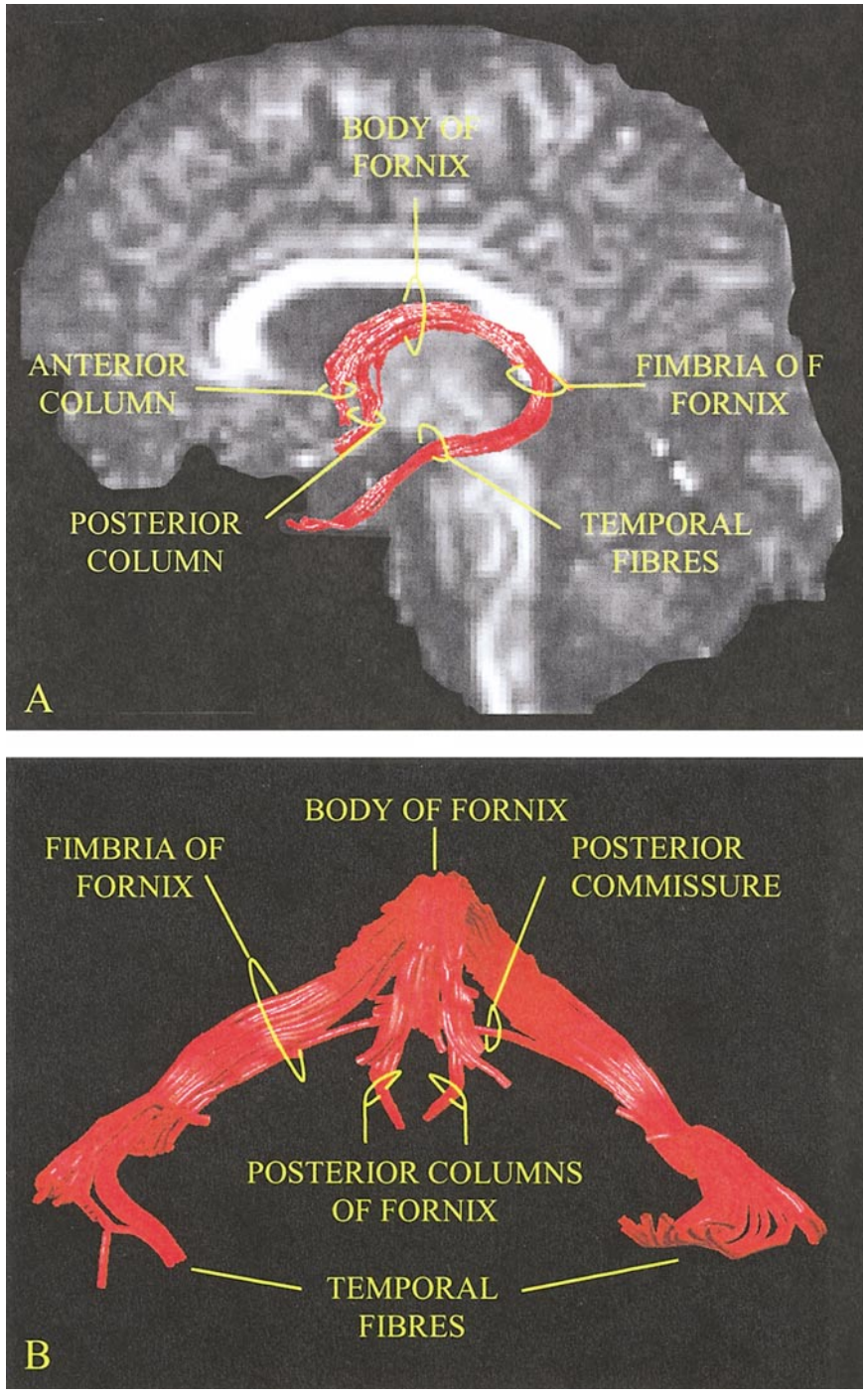

FIG. 13. The fornix is a symmetrical structure of the limbic system connecting the hippocampus with the hypothalamus. The temporal fibers arch supero-posteriorly to form the fimbriae of fornix. A small component of the fimbria crosses contra-laterally (posterior commissure), but the majority of its fibers continue antero-medially into the body of the fornix. The body of the fornix terminates at the hypothalamus as columns (anterior and posterior), but only the posterior columns reach the mammillary bodies. (A) Lateral view of sagittal projection; (B) anterior view of coronal projection.

Projection Fibers

The fornix. The fornix is a limbic structure principally connecting the hippocampus with the hypothalamus, but it also has a small commissural component (Dejerine, 1895, 1901; Nieuwenhuys *et al.*, 1988). Figure 13 shows two views of the reconstructed trajectories obtained in the fornix. Fibers arise from the hippocampus and parahippocampal gyrus of each side and run through the fimbria to join beneath the splenium of

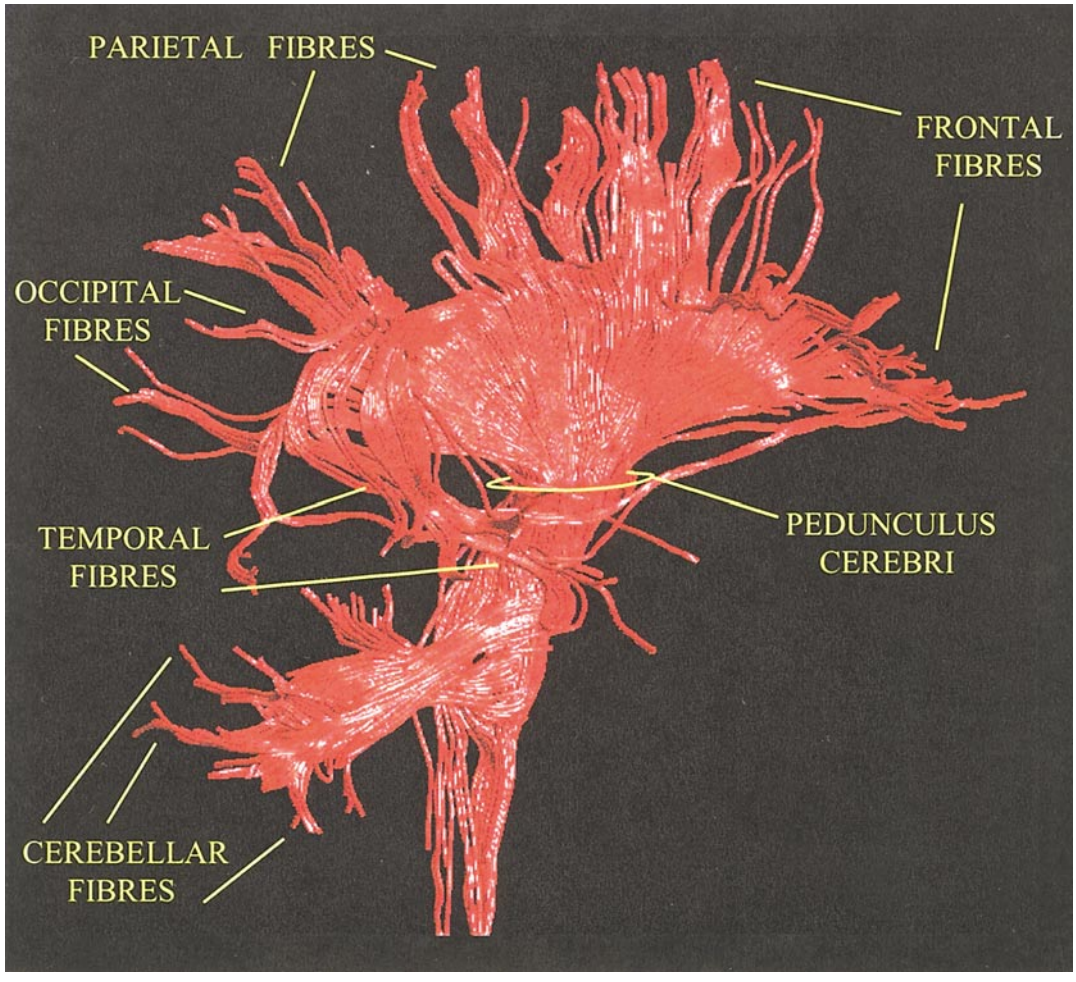

FIG. 14. The internal capsule is composed of fibers running from the cerebral cortex to the midbrain nuclei, cerebellum, and spinal cord (motor projections) and of thalamic fibers running from the cerebellum and spinal cord to the thalamus and from the thalamus to the cerebral cortex. The portion of fibers that runs from the pedunculus cerebri to the cortex forms the corona radiata.

the corpus callosum to form the body of the fornix (Nieuwenhuys *et al.*, 1988; Kiernan, 1998). Other fimbrial fibers continue medially to cross the midline to project to the contralateral parahippocampal gyrus and hippocampus (posterior hippocampal commissure) (Crosby *et al.*, 1962). Most of the fibers within the body of the fornix run anteriorly below the body of the corpus callosum toward the anterior commissure. Above the interventricular foramen, the body of the fornix divides into right and left bundles (Dejerine, 1901; Williams and Worwick, 1980). As each bundle approaches the commissure it diverges again into two components. One of these, the posterior column of the fornix, curves ventrally in front of the interventricular foramen of Monroe and posterior to the anterior commissure to enter the mammillary body of the hypothalamus (postcommissural fornix) (Dejerine, 1901). The second bundle leaves the fornix just above the anterior commissure and enters the hypothalamus as the precommissural anterior column of the fornix (Crosby *et al.*, 1962; Nieuwenhuys *et al.*, 1988; Kiernan, 1998).

The internal capsule. The internal capsule (Fig. 14) is composed of two major components: thalamic radiations and motor projections (England and Wakely, 1991). Thalamic projections radiate anteriorly to frontal cortex, superiorly to parietal cortex, posteriorly to occipital cortex, and inferolaterally to temporal cortex. Motor projections connect fronto-parietal areas with subcortical nuclei (basal ganglia, pontine, and bulbar) and the spinal cord. As the thalamic and motor projections run from the internal capsule to the cortex they form a fan-shaped structure (corona radiata) (Dejerine, 1901). The internal capsule corresponds to the handle of this fan and is bordered by the thalamus and caudate medially and by the lenticular nucleus laterally (Crosby *et al.*, 1962; England and Wakely, 1991). The internal capsule is divided into anterior and posterior limbs that are joined at the genu (Crosby *et al.*, 1962). Within each of these three regions, thalamic and motor projections run together. The anterior limb carries thalamic projections to the frontal lobes and fronto-pontine motor fibers, the genu contains thalamic projec-

tions to the parietal lobe and corticonuclear motor fibers, and the posterior limb contains posterior and inferolateral thalamic projections and corticospinal, corticopontine, and corticotegmental motor fibers (Dejerine, 1901; Williams and Worwick, 1980).

DISCUSSION

We have utilized a tractography algorithm for diffusion tensor imaging data to elucidate the pathways of the major white matter fasciculi in the human brain. The results are faithful to those of classical neuroanatomy studies (e.g., Dejerine, 1895; Crosby *et al.,* 1962) performed with postmortem sectioning. The advantage of the technique demonstrated here is that it is noninvasive, and the results are obtained from data collected within 14 min so that it is possible to obtain similar results from a wide range of subjects.

Since the results obtained here are so similar to those obtained via histological sectioning or dissection, together with the interactive nature of the approach and that all our results have been obtained entirely noninvasively and *in vivo,* we have entitled this approach "virtual *in vivo* interactive dissection," or "VIVID."

In this paper, we have chosen to show data from only one subject—to illustrate the use of the technique. However, in a future paper, we will report findings from a much larger cohort of subjects. Since we submitted this work, we have recently learned of a study by Mori *et al.* (2002) in which a subset of the tracts reconstructed here were studied with an alternative tractography technique (Mori *et al.,* 1999). In this study, the authors appear to have shown consistent results across 10 subjects in mapping a subset of the tracts presented here using DT-MRI, though with a slightly different technique. It is recommended that the reader compare the results presented in the current paper with those by Mori *et al.* (2002) in which striking similarities between reconstructions of tracts such as the superior longitudinal fasciculus can be appreciated. Such comparisons tend to suggest that DT-MRI-based reconstructions of these fibers are reproducible regardless of differences in data acquisition and analysis techniques.

We now wish to highlight several important points with regard to the use of diffusion tensor imaging data as a basis for tractography. First, the data in this study were acquired with resolution of $2.5 \times 2.5 \times 2.5$ mm. Since the diameter of axons is typically 10 μm, it is clear that each voxel can contain a large number of axons. The estimate of orientation of the tensor is therefore an average of the orientations of all the axons contained within the voxel. When the axons are coherently organized in a parallel fashion, the orientation of the tensor will truly reflect the orientation of the underlying fibers. However, when the axons are not oriented in a highly coherent fashion (for example when fibers cross within a voxel), then the voxel-averaged estimate of orientation cannot accurately summarize the orientation of the underlying fibers (Virta *et al.,* 1999). In such voxels, it is clear that there is room for error in tractography (Pierpaoli *et al.,* 2001). Techniques for the analysis of diffusion-weighted MR data that permit more than one orientation to be determined in those voxels containing multi-orientational fiber populations have recently been developed (Tuch *et al.,* 1999; Wedeen *et al.,* 2000; Frank, 2001). The ability to extract different orientations of fibers within such voxels would undoubtedly lead to more accurate tractography results in these areas, and this is the subject of our ongoing research.

A second confounding factor is the effect of noise in the MR imaging system. This serves to add uncertainty to the estimate of the orientation of the tensor (and therefore the fibers) in each voxel. It is clear that a technique that relies on successive estimation of fiber orientation to construct a trajectory could be affected by such problems and spurious pathways could be reconstructed by its use. One may therefore have expected a larger number of "aberrant" trajectories than found in our data. However, adoption of a two-regions of interest approach in this study, so that only those tracts that connect two ROIs were retained, served to "edit out" spurious pathways. For example, those that had been initiated from the correct location, but which had deviated from their correct trajectory due to the effects of noise, would not be displayed. It is also possible that pathways that do connect the two regions, and therefore would have been displayed, had also deviated from the true paths of the underlying fasciculi. This could be the case for the tractography results obtained in the superior fronto-occipital fasciculus, in which posterior fiber trajectories terminated in the parietal lobe, rather than in the occipital lobe. However, among all the fasciculi, this is the most unknown and there is great disagreement about the pathways taken by this fasciculus even in the classical neuroanatomy textbooks (Dejerine, 1895; Crosby *et al.,* 1962; Nieuwenhuys *et al.,* 1988). Since there are no *ad hoc* studies of the anatomy of the fronto-occipital fasciculus performed with more recent techniques, our finding will need to be confirmed in a larger number of subjects. The use of a smoothing procedure as employed here, and described elsewhere by Aldroubi and Basser (1999) and Pajevic *et al.* (2001), served to partly ameliorate the problems of noise. However, it is clear that further validation of the tractography procedure using an independent technique, such as the tract tracing methods outlined in the Introduction, is needed.

Despite the confounding factors outlined above, our results demonstrate that the virtual tract maps obtained using current diffusion tensor tractography approaches are faithful to the classical descriptions of

neuroanatomy that have previously been documented by more invasive means.

CONCLUSION

The aim of this work was to replicate, *in vivo*, the results of classic postmortem studies of the neuroanatomy of white matter fasciculi using diffusion tensor MR tractography. We have demonstrated the use of the technique to map out the 3D trajectories of 10 major white matter fasciculi, where the orientational coherence of constituent fibers is relatively high. The advent of improved imaging hardware (e.g., increased field strengths, increased diffusion-encoding gradient amplitudes) and tracking algorithms which correctly handle the effects of intravoxel averaging of multiorientational fiber populations, should allow us to explore the trajectories of the smaller connections of the brain in more detail in the future and thus allow an atlas of the entire network of connections to be created.

This is the first time that the 3D neuroanatomy of the major white matter fasciculi can be displayed and described, in detail, in living human subjects. Since many diseases of the brain affect the white matter, and this technique allows acquisition of data in only 14 min, the potential of the technique in a clinical setting is clear.

ACKNOWLEDGMENTS

We thank The Wellcome Trust (Grant No. 054030/Z/98/JRS/JP/JAT) who supported this work. Part of this work was made possible through a visit made by D.K.J. to the Section of Tissue Biophysics and Biomimetics, National Institute of Child Health and Human Development, Bethesda, Maryland. We are grateful to Mark Horsfield for his input to software for computation of the diffusion tensor and for the correction of eddy-current-induced image distortions. We also thank the staff of the Neuroimaging Research Department, Institute of Psychiatry, London where the data for this study was collected.

REFERENCES

Aldroubi, A., and Basser, P. J. 1999. Reconstruction of vector and tensor fields from sampled discrete data. *Contemp. Math.* **247:** 1–15.

Axer, H., Berks, G., and Keyserlingk, D. G. V. 2000. Visualization of nerve fiber orientation in gross histological sections of the human brain. *Microsc. Res. Technol.* **51:** 481–492.

Basser, P. J., Matiello, J., and Le Bihan, D. 1994. Estimation of the effective self-diffusion tensor from the NMR spin echo. *J. Magn. Reson. B* **103:** 247–254.

Basser, P. J., and Pierpaoli, C. 1995. Elucidating tissue structure by diffusion tensor MRI. In *Book of Abstracts: Third Annual Meeting of the International Society for Magnetic Resonance in Medicine*, p. 900. ISMRM, Berkeley, CA.

Basser, P. J., and Pierpaoli, C. 1996. Microstructural and physiological features of tissue elucidated by quantitative-diffusion-tensor MRI. *J. Magn. Reson. B* **111:** 209–219.

Basser, P. J. 1998. Fiber-Tractography via diffusion tensor MRI (DT-MRI) In *Book of Abstracts: Sixth Annual Meeting of the International Society for Magnetic Resonance in Medicine,* p. 1226. ISMRM, Berkeley, CA.

Basser, P. J., Pajevic, S., Pierpaoli, C., Duda, J., and Aldroubi, A. 2000. In vivo tractography using DT-MRI data. *Magn. Reson. Med.* **44:** 625–632.

Conturo, T. E., Lori, N. F., Cull, T. S., Akbudak, E., Snyder, A. Z., Shimony, J. S., McKinstry, R. C., Burton, M., and Raichle, M. E. 1999. Tracking neuronal fiber pathways in the living human brain. *Proc. Natl. Acad. Sci. USA* **96:** 10422–10427.

Coremans, J., Luypaert, R., Verhelle, F., Stadnik, T., and Osteaus, M. 1994. A method for myelin fibre orientation mapping using diffusion-weighted MR images. *Magn. Reson. Imag.* **12:** 443–454.

Cowan, W. M., and Cuénod, M. 1975. *The Use of Axonal Transport for Studies of Neuronal Connectivity*. Elsevier, Amsterdam.

Crank, J. 1956. *The Mathematics of Diffusion*. Oxford Univ. Press, Oxford.

Critchley, M. 1996. *The Parietal Lobes*. Hafner, New York.

Crosby, E. C., Humphrey, T., and Lauer, E. W. 1962. *Correlative Anatomy of the Nervous System*. Macmillian Co., New York.

Dejerine, J. 1895. *Anatomie des Centres Nerveux*, Vol. 1, Rueff et Cie, Paris.

Dejerine, J. 1901. *Anatomie des Centres Nerveux*, Vol. 2, Rueff et Cie, Paris.

Demeter, S., Rosene, D. L., and van Hoesen, G. W. 1990. Fields of origin and pathways of the interhemispheric commissures in the temporal lobe of macaques. *J. Comp. Neurol.* **302:** 29–53.

England, M. A., and Wakely, J. 1991. *A Colour Atlas of the Brain and Spinal Cord*. Wolfe, Aylesbury, UK.

Frank, L. R. 2001. Anisotropy in high angular resolution diffusion-weighted MRI. *Magn. Reson. Med.* **45:** 935–939.

Gloor, P. 1997. *The Temporal Lobe and the Limbic System*. Oxford Univ. Press, New York.

Heimer, J., and Robards, M. J. 1981. *Neuroanatomical Tract-Tracing Methods*. Plenum, New York.

Heimer, J., and Záborszky, L. 1989. *Neuroanatomical Tract-Tracing Methods: Recent Progress*. Plenum, New York.

Jones, D. K., Williams, S. C. R., and Horsfield, M. A. 1997. Full representation of white matter fibre direction on one map via diffusion tensor analysis, In *Book of Abstracts: Fifth Annual Meeting of the International Society for Magnetic Resonance in Medicine*, p. 1743. ISMRM, Berkeley, CA.

Jones, D. K., Simmons, A., Williams, S. C. R., and Horsfield, M. A. 1998. Non-invasive assessment of structural connectivity in white matter by diffusion tensor MRI. In *Book of Abstracts: Sixth Annual Meeting of the International Society for Magnetic Resonance in Medicine*. p. 531. ISMRM, Berkeley, CA.

Jones, D. K., Simmons, A., Williams, S. C. R., and Horsfield, M. A. 1999a. Non-invasive assessment of axonal fiber connectivity in the human brain via diffusion tensor MRI. *Magn. Reson. Med.* **42:** 37–41.

Jones, D. K., Horsfield, M. A., and Simmons, A. 1999b. An optimal strategy for precise determination of the diffusion tensor. In *Book of Abstracts: Sixth Annual Meeting of the International Society for Magnetic Resonance in Medicine,* pp. 1793. ISMRM, Berkeley, CA.

Jones, D. K., Horsfield, M. A., and Simmons, A. 1999c. Optimal strategies for measuring diffusion in anisotropic systems by magnetic resonance imaging. *Magn. Reson. Med.* **42:** 515–525.

Jones, D. K., Williams, S. C. R., Gasston, D., Horsfield, M. A., Simmons, A., and Howard, R. 2002. Isotropic resolution diffusion tensor imaging with whole brain acquisition in a clinically acceptable time. *Hum. Brain Mapp.* **15:** 216–230.

Kiernan, J. A. 1998. *Barr's the Human Nervous System: An Anatomical View Point*. Lippincot–Raven, Philadelphia.

Klingler, J., and Gloor, P. 1960. The connections of the amygdala and of the anterior temporal cortex in the human brain. *J. Comp. Neurol.* **115:** 333–369.

Lauer, E. W. 1945. The nuclear pattern and fiber connections of certain basal telencephalic centers in the macaque. *J. Comp. Neurol.* **82:** 215–254.

Lee Seldon, H. 1985. The anatomy of speech perception: Human auditory cortex. In *Cerebral Cortex,* Vol. 4. *Association and Auditory Cortices* (A. Peters and E. G. Jones, Eds.), pp. 273–327. Plenum, New York.

Ludwig, E., and Klingler, J. 1956. *Atlas Cerebri Humani.* S. Karger, Basel.

Mai, J. K., Assheuer J., and Paxinos G. 1997. *Atlas of the Human Brain*. Academic Press, San Diego.

Makris, N., Worth, A. J., Sorenson, A. G., Papadimitriou, G. M., Wu, O., Reese, T. G., Wedeen, V. J., Davis, T. L., Stakes, J. W., Caviness, V. S., Kaplan, E., Rosen, B. R., Pandya, D. N., and Kennedy, D. N. 1997. Morphometry of in vivo human white matter association pathways with diffusion weighted magnetic resonance imaging. *Ann. Neurol.* **42:** 951–962.

Mesulam, M. M., and Mufson, E. J. 1985. The insula of Reil in man and monkey: Architectonics, connectivity, and function. *Cerebral Cortex,* Vol. 4. *Association and Auditory Cortices*. (A. Peters and E. G. Jones, Eds.), pp. 179–226. Plenum, New York.

Mori, S., Crain, B. J., Chacko, V. P., and van Zijl, P. C. 1999. Three dimensional tracking of axonal projections in the brain by magnetic resonance imaging. *Ann. Neurol.* **45:** 265–269.

Mori, S., Kaufmann, W. E., Davatzikos, C., Stieltjes, B., Amodei, L., Fredericksen, K., Pearlson, G. D., Melhem, E. R., Solaiyappan, M., Raymond, G. V., Moser, H. W., and van Zijl, P. C. M. 2002. Imaging cortical association tracts in the human brain using diffusion tensor-based axonal tracking. *Magn. Reson. Med.* **47:** 215–223.

Nakada, H., and Matsuwaza, H. 1995. Three-dimensional anisotropy contrast magnetic resonance imaging of the rat nervous system: MR axonography. *Neurosci. Res.* **22:** 389–398.

Nieuwenhuys, R., Voogd, J., and van Huijzen, C. 1988. *The Human Central Nervous System*. Springer-Verlag, Berlin.

Pajevic, S., and Pierpaoli, C. 1999. Color schemes to represent the orientation of anisotropic tissues from diffusion tensor data: Application to white matter fiber tract mapping in the human brain. *Magn. Reson. Med.* **42:** 526–540.

Pajevic, S., and Pierpaoli, C. 2000. Color schemes to represent the orientation of anisotropic tissues from diffusion tensor data: Application to white matter fiber tract mapping in the human brain. *Magn. Reson. Med.* **43:** 921.

Pajevic, S., Basser, P. J., and Aldroubi, A. 2001. A continuous tensor field approximation for DT-MRI data. In *Book of Abstracts: Seventh Annual Meeting of the International Society for Magnetic Resonance in Medicine,* p. 1535. ISMRM, Berkeley, CA.

Pandya, D. N., and Rosene, D. L. 1985. Some observations on trajectories and topography of commissural fibres. In *Epilepsy and the Corpus Callosum* (A. G. Reeves, Ed.), pp. 21–39. Plenum, New York.

Petrides, M., and Pandya, D. N. 1988. Association fibre pathways to the frontal cortex from the superior temporal in the rhesus monkey. *J. Comp. Neurol.* **283:** 52–66.

Pierpaoli, C., and Basser, P. J. 1996. Towards a quantitative assessment of diffusion anisotropy. *Magn. Reson. Med.* **36:** 893–906.

Pierpaoli, C. 1997. Oh no! One more method for color mapping of fiber tract direction using diffusion MR imaging data. In *Book of Abstracts: Fifth Annual Meeting of the International Society for Magnetic Resonance in Medicine,* p. 1741. ISMRM, Berkeley, CA.

Pierpaoli, C., Barnett A., Pajevic, S., Chen, R., Penix LaRoy, Virta, A., and Basser, P. 2001. Water diffusion changes in Wallerian degeneration and their dependence on white matter architecture. *NeuroImage* **13:** 1174–1185.

Poupon, C., Clark C. A., Frouin, V., Regis, J., Bloch, I., Le Bihan, D., and Mangin, J. 1999. Tracking white matter fasciculi with diffusion tensor imaging. In *Book of Abstracts: Ninth Annual Meeting of the International Society for Magnetic Resonance in Medicine,* p. 325. ISMRM, Berkeley, CA.

Poupon, C., Clark, C. A., Frouin, V., Regis, J., Bloch, I., Le Bihan, D., and Mangin, J. 2000. Regularization of diffusion-based direction maps for the tracking of brain white matter fasciculi. *NeuroImage* **12:** 184–195.

Press, W. H., Teukolsky, S. A., Vetterling, W. T., and Flannery, B. P. 1992. *Numerical Recipes in C: The Art of Scientific Computing.* Cambridge Univ. Press, New York.

Rockland, K. S., and Pandya, D. N. 1986. Topography of occipital lobe commissural connections in the rhesus monkey. *Brain Res.* **365:** 174–178.

Skare, S., Hedehus, M., Moseley, M. E., and Li, T. Q. 2000. Condition number as a measure of noise performance of diffusion tensor data acquisition schemes with MRI. *J. Magn. Reson.* **147:** 340–352.

Stieltjes, B., Kaufmann, W. E., van Zijl, P. C. M., Fredericksen, K., Pearlson, G. D., Solaiyappan, M., and Mori, S. 2001. Diffusion tensor imaging and axonal tracking in the human brainstem. *NeuroImage* **14:** 723–735.

Studholme, C., Hill, D. L. G., and Hawkes, D. J. 1997. Automated three-dimensional registration of magnetic resonance and positron emission tomography brain images by multiresolution optimization of voxel similarity measures. *Med. Phys.* **24:** 25–35.

Tuch, D. S., Weisskoff, R. M., Belliveau, J. W., and Wedeen, V. J. 1999. High angular resolution diffusion imaging of the human brain. In *Book of Abstracts: Seventh Annual Meeting of the International Society for Magnetic Resonance in Medicine,* p. 321. ISMRM, Berkeley, CA.

Turner, B. H., Mishkin, M., and Knapp, M. E. 1979. Distribution of the anterior commissure to the amygdaloid complex in the monkey. *Brain Res.* **162:** 331–337.

Tusa, R. J., and Ungerleider, L. G. 1985. The inferior longitudinal fasciculus: A reexamination in humans and monkeys. *Ann. Neurol.* **18:** 583–591.

Ulug, A. M. O., Bakht, O., Bryan, R. N., and van Zijl, P. C. M. 1996. Mapping of human brain fibers using diffusion tensor imaging. In *Book of Abstracts: Fourth Annual Meeting of the International Society for Magnetic Resonance in Medicine,* p. 1325. ISMRM, Berkeley, CA.

Di Virgilio, G., Clarke, S., Pizzolato, G., and Schaffner, T. 1999. Cortical regions contributing to the anterior commissure in man. *Exp. Brain Res.* **124:** 1–7.

Virta, A., Barnett, A., and Pierpaoli, C. 1999. Visualizing and characterizing white matter fiber structure and architecture in the human pyramidal tract using diffusion tensor MRI. *Magn. Reson. Imag.* **17:** 1121–1133.

Wedeen, V. J., Reese, T. G., Tuch, D. S., Weigel, M. R., Dou J-G., Weisskoff, R. M., and Chesler, D. 2000. Mapping fiber orientation spectra in cerebral white matter with Fourier transform diffusion MRI. In *Book of Abstracts: Eighth Annual Meeting of the International Society for Magnetic Resonance in Medicine,* p. 82. ISMRM, Berkeley, CA.

Williams, P. L., and Worwick, R. 1980. *Gray's anatomy*. Churchill, Edinburgh/London.

Zhang, S., Curry, C., Morris, D. S., and Laidlaw, D. H. 2000. Visualizing diffusion tensor MR images using streamtubes and streamsurfaces. *Proceedings of the IEEE Visualization Conference,* Utah.